J. Fluid Mech. (1970), *vol.* 43, *part* 2, *pp.* 291–303
Printed in Great Britain

Statistical properties of turbulent density fluctuations

By L. N. WILSON AND R. J. DAMKEVALA
IIT Research Institute, Chicago, Illinois

(Received 12 September 1969)

The cross-correlation technique has been used to obtain statistical properties of scalar density fluctuations. Two schlieren instruments with their optical beams intersecting in the turbulent field each give a signal proportional to the density gradient in the flow direction but integrated along the beam path. Cross-correlation of the two signals gives an area integral of the density-gradient covariance. For locally isotropic conditions the area integration can exactly compensate for the two gradients giving a result proportional to the local mean-square density fluctuation at the beam intersection point.

Experiments performed in the shear layer of a subsonic jet show results which tend to verify the principles of crossed-schlieren measurement. Intensity levels are close to those predicted assuming density fluctuations are related isentropically to local, incompressible pressure fluctuations.

1. Introduction

Studies of scalar turbulent fields have been limited almost entirely to the analysis of mixing processes. This is a result of the difficulty of obtaining direct experimental measurements of scalar quantities like temperature, density or concentration at points within the flow. Some indirect measurements have been reported by Kistler, O'Brien & Corrsin (1954) using hot wire techniques, operating under conditions where the wire was sensitive to both temperature and velocity. It was then necessary to separate the effects of the two (scalar and vector) fields. More recently a new technique, the crossed-beam correlation technique, was developed by Fisher & Krause (1967) which measures the light scattered from two optical beams crossed in the region of interest in a turbulent air jet. By cross-correlating the signals from each beam, local information on the statistical behaviour of scatterer number-density in the vicinity of the intersection point was extracted. Unfortunately it was necessary to seed the flow with artificial scatterers to give sufficient signal levels and therefore the results could not be related directly to a local scalar property of the air. In principle, the technique can use absorption by a flow constituent to give the required signal which can be related to its temperature and density. However, not only is the relation in general a complicated one, but most fluids of interest, in particular air, have no strong absorbers in the visible portion of the spectrum. Moreover, in order to obtain local fluctuation level estimates using either scattering or absorption it is necessary to estimate turbulent scale lengths along the beam directions.

The present study employs the crossed-beam correlation technique in a manner designed to give the local refractive index fluctuations from which mass-density fluctuations can be inferred directly, both being local properties of the fluid. The refractive-index changes are monitored by using the crossed-beam as a schlieren instrument, the signals obtained then being a measure of refractive-index gradients. Since crossed-beam geometry results in an area integral in the cross-flow direction, these gradients tend to be integrated out and no independent scale-length estimates are then required. The underlying analysis required and some experimental results are given in subsequent sections.

2. Crossed-beam schlieren instrument

The basic operation of a crossed-beam schlieren instrument is best described by reference to figure 1. Two collimated beams of light, A and B, parallel to the Y and Z axes respectively, pass through the flow normal to the flow direction X. The beams are separated a distance ξ along the flow direction. Each beam is focused on a detector after being partially cut off by a knife edge placed perpendicular to the flow direction. In this configuration, the signal at the detector in each case is proportional to the refractive-index gradient in the X direction.

A refractive-index gradient in the X direction causes the beam to bend a small angle θ, with the result that the beam moves normal to the knife edge a distance $l\theta$ causing the light intensity on the detector to change a proportional amount. l is the distance from the disturbance to the knife edge.

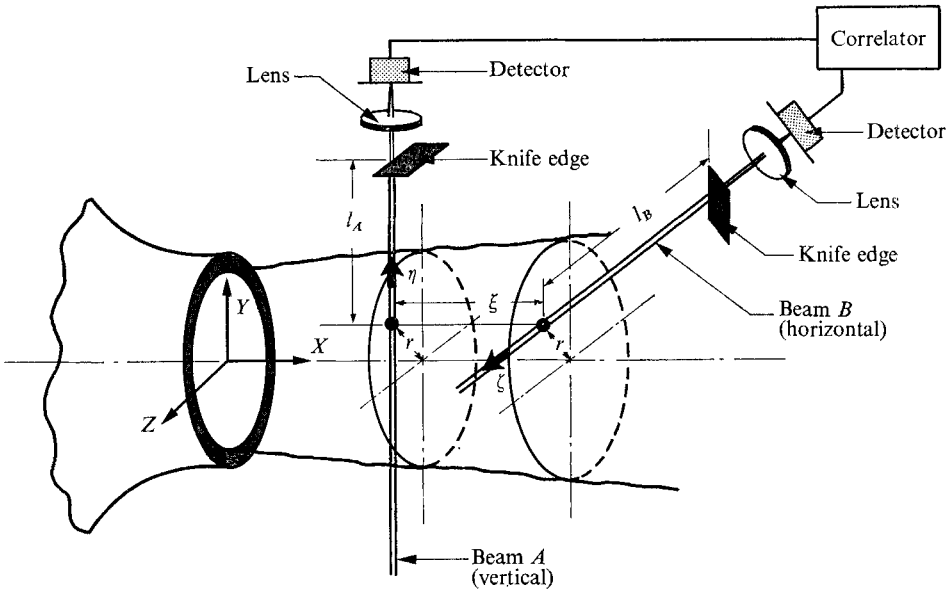

FIGURE 1. Sketch showing arrangement and co-ordinate axes for discussion of crossed-beam schlieren instrument.

These schlieren systems are somewhat unconventional in that they employ lenses only past the knife edges, their purpose being to prevent overfilling the

detectors and to simplify alignment. No attempt is made to make the systems particularly sensitive. The reason for this is that a circular cross-section beam was used and if the signals measured are to be directly proportional to refractive index gradients, the movement $l\theta$ must be much smaller than the beam diameter d. In this mode of operation the distance l from the disturbance to the knife edge is not usually constant so that more distant points in the flow are weighted more heavily. After cross-correlation of the signals the effect is small as long as l is always much larger than correlated lengths within the flow. It should further be pointed out here, that fluctuations whose scales are smaller than the beam diameter are not properly resolved. This gives an upper limit to the frequencies which can be measured, and is typically above 30 kHz for the nominal 1 mm beams used in the present study.

If the mean signal measured on the photodetector is E and a deflexion θ causes a change in signal of e, then, theory of schlieren operation, covered for example by Liepmann & Roshko (1957) gives $e = Sl\theta$ where S is the schlieren sensitivity. For a linear response S is a constant of the system, and for a logarithmic response $S = \sigma E$, where $\sigma = 8l/\pi d$ for a circular beam. Continuous measurement of e then allows us to determine the deflexion history of θ integrated along each beam. It now remains to relate these signals to the refractive-index and density changes and show how the information in the region of beam intersection can be extracted.

3. Analytical background

A light ray, passing through a medium of variable refractive index is deflected (see for example, Born & Wolf 1959) according to

$$\Theta = \int_0^L \left(\mathbf{n}.\,\frac{1}{N}\operatorname{grad} N\right) d\mathbf{s}, \tag{1}$$

where Θ is the deflexion angle along a light path $\mathbf{s}$ integrated over a distance L, $\mathbf{n}$ is the unit vector normal to $\mathbf{s}$ and N is the index of refraction, assumed to be comprised of an ambient value N_0, a local mean change n_0 relative to ambient and a local fluctuating part n, such that $N = N_0 + n_0 + n$.

In the reference frame of the crossed-beam schlieren instrument, with knife edges oriented as shown in figure 1, we may approximate this angle for beam A by

$$\Theta_A(t) = \int_0^{L_y} \frac{1}{N_0[1+(n_0+n)/N_0]} \frac{\partial(N_0+n_0+n)}{\partial x} dy. \tag{2}$$

Assuming that n, n_0 both are much less than N_0, then

$$\Theta_A(t) \simeq \frac{1}{N_0}\int_0^{L_y} \frac{\partial n_0}{\partial x} dy + \frac{1}{N_0}\int_0^{L_y} \frac{\partial n}{\partial x} dy,$$

and a similar expression can be written for the other beam

$$\Theta_B(t) \simeq \frac{1}{N_0}\int_0^{L_z} \frac{\partial n_0}{\partial x} dz + \frac{1}{N_0}\int_0^{L_z} \frac{\partial n}{\partial x} dz. \tag{3}$$

The first terms of these expressions represent the mean beam deflexion θ_0 and the second the fluctuating deflexion $\theta(t)$.

Multiplying Θ_A by Θ_B and averaging over a long time interval we obtain, for stationary conditions:

$$\langle \theta_A \theta_B \rangle = \frac{1}{N_0^2} \int_0^{L_y} \int_0^{L_z} \left\langle \left(\frac{\partial n}{\partial x}\right)_y \left(\frac{\partial n}{\partial x}\right)_z \right\rangle dy\, dz. \tag{4}$$

This can be related to the a.c. coupled schlieren-detector outputs e_A and e_B

$$\langle \theta_A \theta_B \rangle = \frac{\langle e_A e_B \rangle}{S_A S_B l_A l_B}. \tag{5}$$

The refractive index of a gas can be related to its density through

$$N - 1 = \alpha \Gamma,$$

where α is the Gladstone–Dale constant, a property of the gas and a function of the wavelength of the light source.

Assuming Γ, the density, to be separable into the ambient value Γ_0, a mean change ρ_0 relative to ambient and a fluctuation ρ, so that

$$\Gamma = \Gamma_0 + \rho_0 + \rho,$$

then

$$\frac{\partial n}{\partial x} = \alpha \frac{\partial \rho}{\partial x}.$$

Transforming to axes ξ, η, ζ centred at the beam intersection point x, y, z and defining a crossed-beam covariance, Q_s we then obtain

$$\frac{\langle e_A e_B \rangle N_0^2}{S_A S_B l_A l_B \alpha^2} = Q_s(\xi, x, y, z) = \int_{-\frac{1}{2}L_y}^{\frac{1}{2}L_y} \int_{-\frac{1}{2}L_z}^{\frac{1}{2}L_z} \left\langle \frac{\partial \rho(x, y+\eta, z)}{\partial x} \frac{\partial \rho(x+\xi, y, z+\zeta)}{\partial x} \right\rangle d\eta\, d\zeta. \tag{6}$$

At this stage, it is necessary in order to proceed further to assume that the turbulence is homogeneous over distances for which the covariance in the integrand of (6) contributes appreciably to the integral. This allows two simplifications of the equation: (i) the integration limits may be extended to include $-\infty$ to $+\infty$ for both variables; (ii) the integrand may be replaced by

$$\left\langle \frac{\partial \rho(x, y+\eta, z)}{\partial x} \frac{\partial \rho(x+\xi, y, z+\zeta)}{\partial x} \right\rangle = -\frac{\partial^2}{\partial \xi^2} \langle \rho(x, y, z)\, \rho(x+\xi, y+\eta, z+\zeta) \rangle$$

$$= -\frac{\partial^2}{\partial \xi^2} Q(\xi, \eta, \zeta),$$

where $Q(\xi, \eta, \zeta)$ is the two-point density covariance.

Then equation (6) becomes simply

$$Q_s(\xi) = -\int\int_{-\infty}^{+\infty} \frac{\partial^2 Q(\xi, \eta, \zeta)}{\partial \xi^2} d\eta\, d\zeta. \tag{7}$$

In order to understand more clearly what Q_s represents, we can perform a one-dimensional Fourier transform of (7), and obtain the experimentally accessible schlieren 'energy' spectrum $E_s(\kappa_x)$,

$$E_s(\kappa_x) = \frac{1}{8\pi^3} \int_{-\infty}^{\infty} Q_s(\xi) \exp(-i\kappa_x \xi)\, d\xi$$

$$= \frac{-1}{8\pi^3} \int\int\int_{-\infty}^{\infty} \frac{\partial^2 Q(\xi, \eta, \zeta)}{\partial \xi^2} \exp(-i\kappa_x \xi)\, d\xi\, d\eta\, d\zeta, \tag{8}$$

where κ_x is the X component of wave-number.

This may be integrated by parts twice with respect to ξ to give

$$E_s(\kappa_x) = \frac{\kappa_x^2}{8\pi^3}\int\int\int_{-\infty}^{\infty} Q(\xi,\eta,\zeta)\exp(-i\kappa_x\xi)\,d\xi\,d\eta\,d\zeta. \tag{9}$$

The three-dimensional energy spectrum for a scalar quantity is given by

$$E_3(\kappa_x,\kappa_y,\kappa_z) = \frac{1}{8\pi^3}\int\int\int_{-\infty}^{\infty} Q(\xi,\eta,\zeta)\exp[-i(\kappa_x\xi+\kappa_y\eta+\kappa_z\zeta)]\,d\xi\,d\eta\,d\zeta,$$

from which

$$E_3(\kappa_x,0,0) = \frac{1}{8\pi^3}\int\int\int_{-\infty}^{\infty} Q(\xi,\eta,\zeta)\exp(-i\kappa_x\xi)\,d\xi\,d\eta\,d\zeta.$$

Combining this with (9)

$$E_s(\kappa_x) = \kappa_x^2 E_3(\kappa_x,0,0). \tag{10}$$

That is, the crossed-beam schlieren system gives, in locally homogeneous flow, a spectrum which is κ_x^2 times the one-dimensional (streamwise) component of the three-dimensional spectrum.

The ability of the crossed-beam to measure a three-dimensional spectrum directly has been noted before (Wilson *et al.* 1969) and is distinct from the two-point measurements (e.g. hot wire) which determine the so-called one-dimensional spectrum. The spectrum E_s represents the classical energy spectrum function and will exhibit a peak with wave-number rather than remaining flat at small wave-numbers as is the case for two-point measurements. The peak for E_s will in fact occur at a wave-number corresponding to the scale of the main energy containing eddies, whereas the peak of E_3 would occur at a somewhat smaller wave-number, corresponding to the main convection or diffusion eddies.

The two-point covariance Q can be obtained directly from measurements of Q_s if we make a further restrictive assumption that the turbulence is locally isotropic within volumes corresponding to the range of the homogeneous assumption. Then we can rewrite (7) as

$$Q_s(\xi) = -2\pi\int_{\xi}^{\infty}\frac{d^2Q(r)}{d\xi^2}\,r\,dr, \tag{11}$$

where $r^2 = \xi^2+\eta^2$. Now

$$\frac{d^2Q}{d\xi^2} = \frac{\xi^2}{r^2}\frac{d^2Q}{dr^2}+\frac{1}{r}\left(1-\frac{\xi^2}{r^2}\right)\frac{dQ}{dr}$$

for isotropic conditions and substituting this in (11) we finally obtain

$$Q_s(\xi) = 2\pi\frac{d\xi Q(\xi)}{d\xi}. \tag{12}$$

From this $$Q_s(0) = 2\pi Q(0) = 2\pi\langle\rho^2\rangle$$

or $$\langle\rho^2\rangle = \frac{Q_s(0)}{2\pi} \tag{13}$$

and $$Q(\xi) = \frac{1}{2\pi\xi}\int_0^{\xi} Q_s(\xi')\,d\xi'. \tag{14}$$

These give the very useful results that (i) the mean square density is directly proportional to the schlieren covariance obtained at zero beam separation and

(ii) the two-point density covariance can be obtained by a simple integration of the schlieren covariance with beam separation.

The first result could be predicted intuitively from (7) by observing that for isotropic conditions the double integration will counteract the double differentiation for $\xi = 0$, and scale lengths in the η and ζ directions are no longer important as mentioned earlier. Since the integrand of (6) involves density derivatives, the length scales are reduced and the isotropy condition may not be too severe.

Some preliminary measurements using these crossed-schlieren concepts are presented in the following section.

4. Experiments

A photograph of the crossed-schlieren instrument is reproduced as figure 2, plate 1. Two Quantum Physics model LS 32 helium–neon lasers were used as light sources and EG and G Type SGD-100 photodiodes as detectors. Detectors and lasers were separately mounted on mill traverses, which were adjustable in axial and radial directions relative to the jet. The beams were always moved an equal amount so that each passed through an equal length in the jet. Light was focused into the detectors using $f/3{\cdot}4$ lenses, and the schlieren knife edges were placed to intercept the beams before entering the lenses.

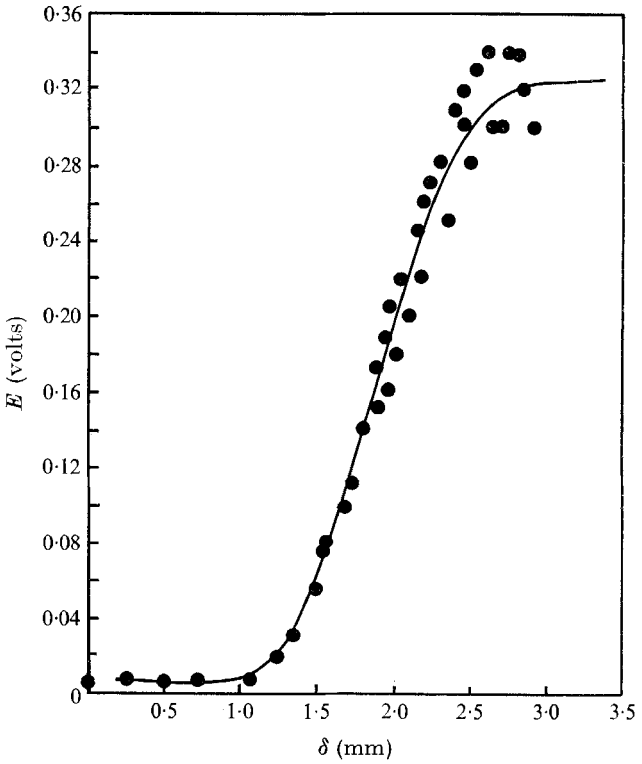

FIGURE 3. Combined calibration curves for schlieren instruments. Sensitivity $S = dE/d\delta$.

Signals from the detectors were recorded on a F.M. tape recorder (Ampex FR 1300) after amplification in the frequency range 300 Hz to 25 kHz. Increasing the upper frequency to 100 kHz made no observable difference to the level of cross-covariances but did increase the single beam autocovariance levels and apparent bandpasses. The latter increases were the result of increased instrument and light source noise. A correlator (PAR Model 101) was used for both on-line monitoring as well as calculation of cross-covariances from the taped data. Integration times of 5 sec were used throughout in determining covariances.

Measurements were made in the shear layer of a 2·54 cm jet operating at nominal efflux speeds of 105 and 210 m/s. For comparison purposes, hot-wire measurements (Thermo-Systems model 1010 A with a model 1005 B linearizer) were made at the lower speed setting.

The sensitivity S, of each schlieren system was determined by measuring the d.c. detector ouput E as a function of knife edge position δ. Typical plots for the two systems are given in figure 3 where we see that the slope $S = dE/d\delta$ is nearly a constant, at least within a total movement of 1 mm. Thus we may take the constant slope of these curves as the schlieren sensitivity S defined earlier. The dynamic range is then limited to deflexions of less than 1 mm however, and this limitation is checked later. The distance l from the knife edge to the disturbance was measured for each setting of the beams and α was taken as 0·243 cc/g throughout in analysis of the data.

5. Results and discussion

A typical set of covariances is reproduced in figure 4, giving the autocovariance for each beam ($\langle e_A^2 \rangle$, $\langle e_B^2 \rangle$) as well as the cross-covariance between beams ($\langle e_A e_B \rangle$). The ratio

$$\langle e_A e_B \rangle / [\langle e_A^2 \rangle \langle e_B^2 \rangle]^{\frac{1}{2}}$$

is a measure of the mean-square signal to total noise (instrument plus uncorrelated flow noise). For the example of figure 4 this is about 0·25; a rather high value compared with previous crossed-beam studies where signals as low as 0·05 of total noise have been successfully extracted.

The analysis leading to (14) assumed that cross-covariances were measured with a physical space variable ξ, whereas in practice it is more convenient to measure and analyze cross-covariances with a time-delay as variable. This in fact has been done in presenting the data of figure 4. The extent to which the two are relatable was determined by measuring convection speed U_c and relating the space and time variable by $\xi = U_c\tau$ and making measurements for both ξ and τ variations. The results of such measurements $Q_s(\xi, \tau)$, at $x/D = 3$, $y/D = 0{\cdot}5$, are plotted in figure 5 with ξ as a parameter. The time covariance curves decay with increasing ξ as shown. The envelope of the curves is the Lagrangian covariance indicating the decay of turbulence following the eddies which move at the mean convection speed. The time delays and spacings representing the points of tangency between the Lagrangian and Eulerian covariances can be plotted as in figure 5 to obtain the convection speed U_c (140 m/sec).

The results may also be plotted as two separate curves $Q_s(\xi)$ and $Q_s(U_c\tau)$ as

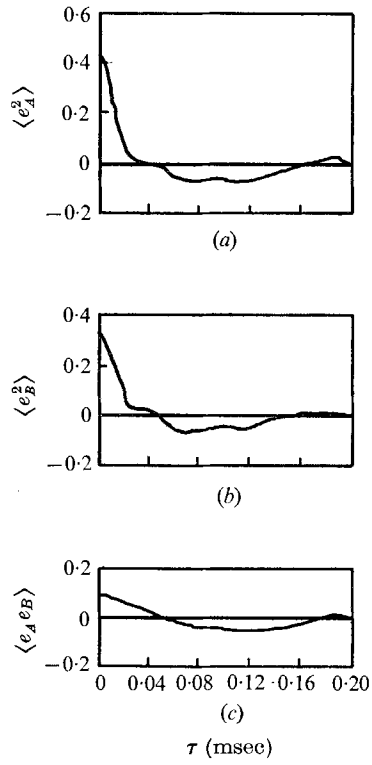

FIGURE 4. Typical correlograms (*a*) vertical beam autocovariance, (*b*) horizontal beam autocovariance, (*c*) two-beam cross-covariance. Arbitrary vertical scales.

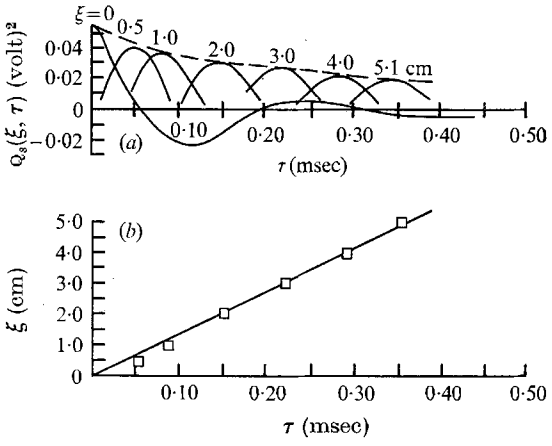

FIGURE 5. Turbulence convection measurements $y/D = 0{\cdot}5$, $x/D = 3{\cdot}0$, $U(0) = 210$ m/sec. (*a*) Space-time covariances. (*b*) Plot of beam separation distance ξ *vs.* corresponding time delay for peak covariance. Slope of solid line is $U_c = 140$ m/sec.

in figure 6. The damped sine-wave shape of the covariances is typical of a peaked shape to the corresponding energy spectra (e.g. by Fourier transform of Q_s) such as we expect for three-dimensional spectra. The peak of the energy spectrum should occur at the frequency (or wave-number) corresponding to the dominant frequency of the covariance. This latter frequency from figure 6 is about $f_p = 5\,\text{kHz}$ (or wave-number of $\kappa_p = 35\,\text{per m}$). We note that the periods of $Q_s(\xi)$ and $Q_s(U_c\tau)$ are identical so that the main eddy contribution is obtained with either the space or time covariance. There is some small decrease in amplitude of the space-covariance for large separations, reflecting the finite turbulence decay or departure from 'frozen' turbulence conditions. The agreement between the two is in general good, however, and we are justified in accepting Taylor's hypothesis and using the transformation $\xi = U_c\tau$, in which case (14) becomes

$$Q(\tau) = \frac{1}{2\pi\tau}\int_0^{\tau} Q_s(\tau')\,d\tau'. \tag{15}$$

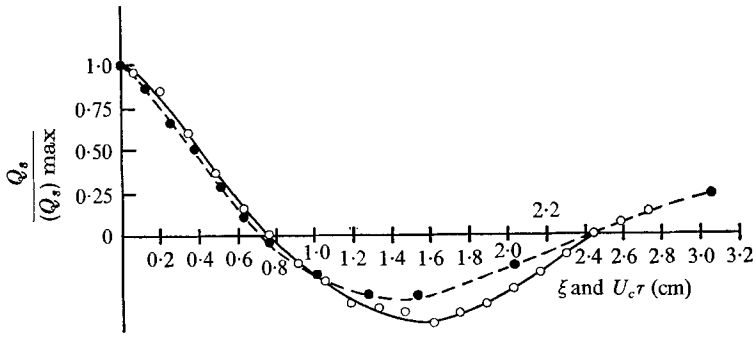

FIGURE 6. Comparison of (●) space covariances, $Q_s(\xi)$ and (○) time covariances $Q_s(U_c\tau)$ $y/D = 0{\cdot}5$, $x/D = 3{\cdot}0$, $U_c = 140$ m/sec.

A comparison of the covariance curves as obtained by hot-wire and crossed-schlieren measurement is presented in figure 7 for $U_0 = 105\,\text{m/sec}$. The higher frequencies associated with the schlieren measurement are evidenced by the short period of its covariance. After integration according to (15) (using a planimeter) however, the period becomes almost identical to that of the hot wire. In fact the two curves for the two-point covariance $Q(\tau)$, i.e. by hot-wire and by crossed-beam measurement are the same within the accuracy expected. The agreement gives strong support to our confidence in the assumptions leading to (14) or (15).

Turbulence intensity measurements are presented in figure 8. Crossed-schlieren measurements with $\xi = 0$ are given for $x/D = 3$ at the two jet efflux speeds. The data on the ordinate are normalized by the change in density $\rho_0(0)$ across the jet shear layer calculated assuming isentropic expansion from the reservoir with the similarity parameter $\lambda = (y - \frac{1}{2}D)/x$ as the abscissa. Since the jet stagnation temperature and the outside ambient temperature were equal to within 2 °C, the isentropic approximation should be good in the 'potential core' of the jet. The calculation of $\rho_0(0)$ assumes pressure constant across the jet exit plane. Also included in figure 8 are hot-wire measurements at the lower

speed. Probe interference effects made measurements at the higher speed impractical. The profiles are all similar in shape, peaking near the centre of the shear layer ($\lambda = 0$), but the levels are not identical; in general the normalized density fluctuations are larger than the corresponding velocity fluctuations.

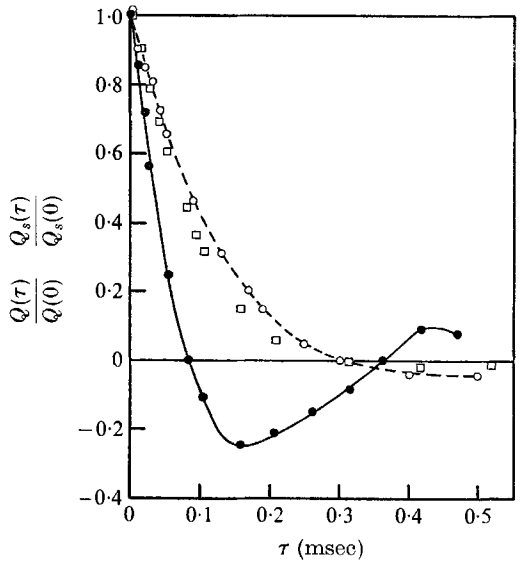

FIGURE 7. Comparison of hot-wire and schlieren covariances. ●, measured crossed-schlieren Q_s; ○, measured hot-wire Q; □, two-point density covariance from Q_s and equation (15).

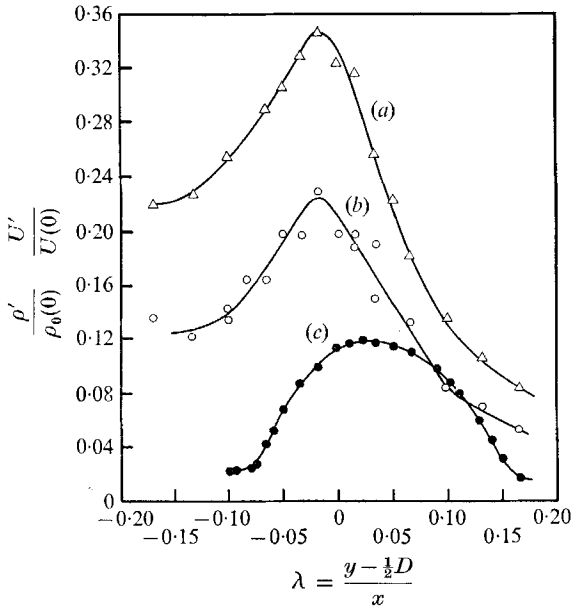

FIGURE 8. Turbulence root-mean-square crossed-schlieren density (ρ') and hot-wire velocity (u') profiles. (*a*) Density fluctuations at $U(0) = 210$ m/sec. (*b*) Density fluctuations at $U(0) = 105$ m/sec. (*c*) Velocity fluctuations at 105 m/sec.

If we consider density changes ρ in the flow direction as being isentropically related to pressure changes p by $\rho = p/C^2(y)$ where C is the local speed of sound, then the density change is related to velocity changes u in the flow direction by the one-dimensional linearized momentum equation:

$$C^2(y)\,\rho'(y) = (\Gamma_0 + \rho_0(y))\,U(y)\,u'(y),$$

where primes refer to root-mean-square values.

Assuming isentropic expansion from ambient temperature (subscript a) to centreline temperature and that density variations across the jet are inversely proportional to temperature T,

$$\frac{\rho_0(0)+\Gamma_0}{\Gamma_0} = \frac{T_a}{T(0)} = 1 + \frac{0{\cdot}2U^2(0)}{C^2(0)}.$$

$\rho_0(0)$, $T(0)$, $U(0)$ refer to conditions in the jet potential core at $y = 0$.

$$\frac{\rho_0(y)+\Gamma_0}{\Gamma_0} = \frac{T_a}{T(y)} \quad \text{and} \quad \frac{C^2(0)}{C^2(y)} = \frac{T(0)}{T(y)}.$$

This gives

$$\frac{\rho'(y)}{\rho_0(0)} = \frac{5U(y)}{U(0)}\,\frac{u'(y)}{U(0)}\left[\left(\frac{T_a}{T(y)}\right)^2 \frac{1}{1+0{\cdot}2[U(0)^2/C(0)^2]}\right]. \tag{16}$$

For $[U(0)/C(0)]^2 < 0{\cdot}5$, as is the case for the present study, the term in the square bracket can be neglected with an error of no more than 10 %. Hence

$$\frac{\rho'(y)}{\rho_0(0)} \cong 5\,\frac{U(y)}{U(0)}\,\frac{u'(y)}{U(0)}. \tag{17}$$

Using the mean velocity profile from Davies, Fisher & Barratt (1963), and the measured r.m.s velocity profile from figure 8, a r.m.s. density profile can be calculated according to (17). Figure 9 shows a comparison between the calculated profile and the profile measured by the schlieren crossed-beam. Although the r.m.s. velocity profile peaks in the region outside the centre of the shear layer ($\lambda > 0$) both the predicted and measured r.m.s. density profiles peak at $\lambda < 0$. Although hot-wire measurements result in a predicted density fluctuation level 50 % higher than measured by the crossed-schlieren, the agreement is gratifying when we consider that for speeds above 100 m/s compressibility effects will alter the hot-wire results. No corrections for compressibility have been taken into account. Within the accuracy of the assumptions, it appears that the density fluctuations are related isentropically to the pressure fluctuations which in turn are driven by inertial fluctuations.

The density levels of figure 8 correspond to a root-mean-square beam-deflexion, at the knife edge of less than 0·05 mm. The assumed constancy of the sensitivity is therefore justified.

Convection speeds were measured for the $U_0 = 210$ m/s condition as in figure 5, and these are plotted in figure 10. The remarkable observation there is that the convection speed is independent of radial distance. Hot-wire results show a tendency for convection speeds to vary slowly across the shear layer but they do drop about a factor of 2 between $\lambda = 0$ and $\lambda = 0{\cdot}10$. The reason for the present observation is not understood at present but tentatively we might suggest that

the schlieren system is sensitive to the sharp density gradients of the jet edge and we therefore tend to measure the phase speed of the growth and decay of large entrainment eddies. As suggested to the authors we may also be measuring the phase speed of instabilities generated in the inflexion region. It has been proposed that such instabilities are responsible for the transfer of energy from the mean flow to the turbulence (see, for example, Kline 1969).

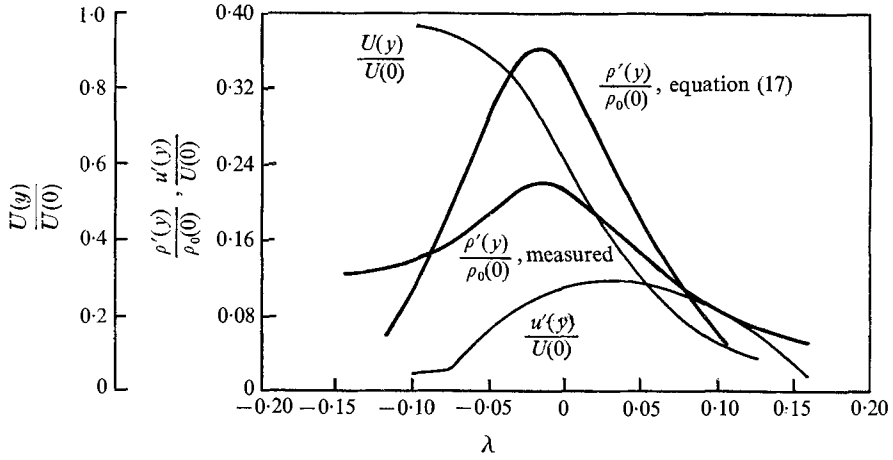

FIGURE 9. Comparison of measured $\rho'(y)$ with $\rho'(y)$ calculated from $u'(y)$ using equation (17).

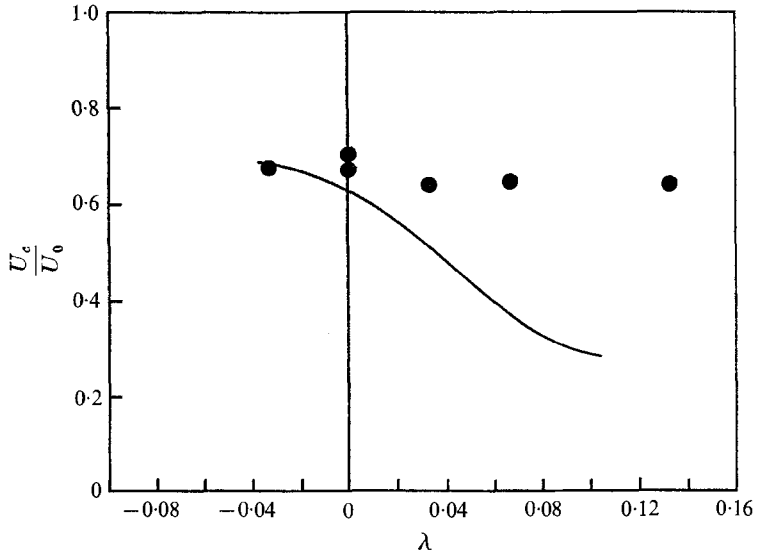

FIGURE 10. Convection speed profiles, $X/D = 3{\cdot}0$, $U(0) = 210$ m/sec. ●, crossed-schlieren results; ——, hot-wire results.

The large difference between convection speed and mean speed near the jet edge may indicate that Taylor's hypothesis and consequently (15) cannot be

justified in that region. However, even if this is so the intensity profiles as determined by (13) do not involve this hypothesis and should be valid.

6. Concluding remarks

The preliminary experiments presented here support the prediction that optical cross-correlation techniques can be used with schlieren instruments to obtain density fluctuation statistics in turbulent flows. The jet shear layer used for the studies presents a rather severe test for the technique since a direct determination of density fluctuations does require the assumption of local isotropy.

Although a more complete assessment of this still must be made the success obtained in these preliminary measurements should give confidence in application of the technique to a broad variety of turbulent flows with smaller shear gradients.

The work presented here was supported in part by the Commercial Airplane Division of the Boeing Airplane Company, Seattle, Washington.

REFERENCES

BORN, M. & WOLF, E. 1959 *Principles of Optics*. New York: Pergamon.

DAVIES, P. O. A. L., FISHER, M. J. & BARRATT, M. J. 1963 *J. Fluid Mech.* **15**, 337.

KISTLER, A. L., O'BRIEN, V. & CORRSIN, S. 1954 *NACA Res. Memo* no. RM54d19.

KLINE, S. J. 1969 Turbulent boundary layer prediction and structure—the state of the art. *Report MD-23, Stanford University.*

FISHER, M. J. & KRAUSE, F. R. 1967 *J. Fluid Mech.* **28**, 705.

LIEPMANN, H. W. & ROSHKO, A. 1957 *Elements of Gas Dynamics*. London: Wiley.

WILSON, L. N., KRAUSE, F. R. & KADRMAS, K. A. 1969 In *Basic Aerodynamic Noise Research* (ed. I. R. Schwarz). *NASA SP-207.*

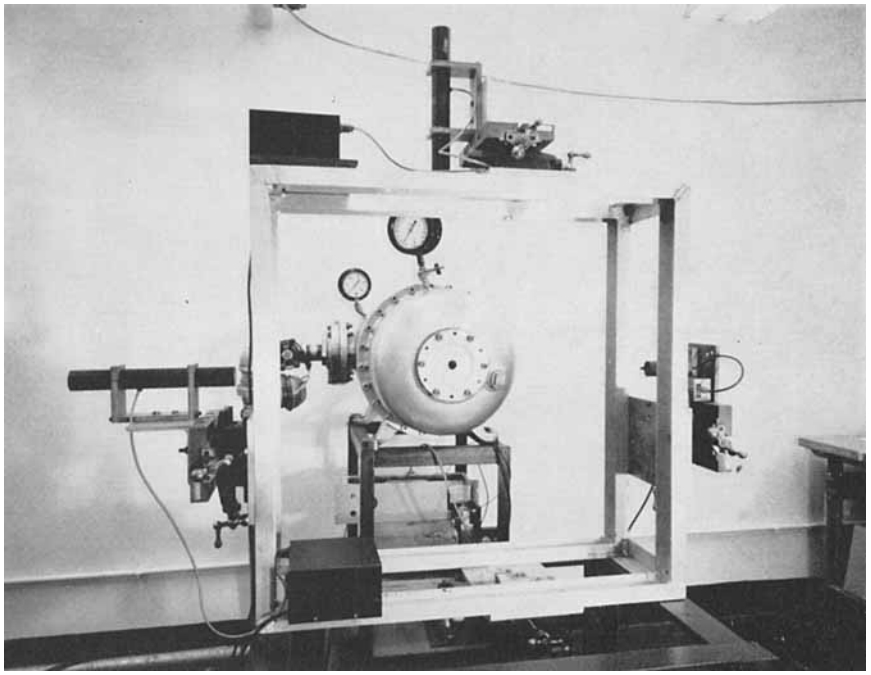

FIGURE 2. Photograph of crossed-schlieren instrument mounted around 2·54 cm jet.